*International Journal of Microwave and Wireless Technologies*

**cambridge.org/mrf**

# Design of a wideband highly efficient GaN HEMT power amplifier for multiband applications

Xuefei Xuan[1,2], Zhiqun Cheng[1], Zhiwei Zhang[1], Tingwei Gong[1] and Chao Le[1]

[1]The School of Electronics and Information, Hangzhou Dianzi University, Hangzhou, China and [2]The School of Electronic Engineering, Huainan Normal University, Huainan, China

**Research Paper**

**Cite this article:** Xuan X, Cheng Z, Zhang Z, Gong T, Le C (2023). Design of a wideband highly efficient GaN HEMT power amplifier for multiband applications. *International Journal of Microwave and Wireless Technologies* **15**, 1468–1474. https://doi.org/10.1017/S1759078723000314

Received: 29 November 2022
Revised: 11 March 2023
Accepted: 14 March 2023

**Keywords:**
distributed matching network; GaN HEMT power amplifiers; highly efficient; left-rotating T-type structure; wideband

**Corresponding author:** Zhiqun Cheng; Email: zhiqun@hdu.edu.cn;
Zhiwei Zhang; Email: 2361051379@qq.com

**Abstract**

A distributed basic matching network (MN) designed method that can achieve multioctave bandwidth and highly efficient power amplifier (PA) for multiband applications is presented in this letter. The distributed network unit with a left-rotating T-type structure is employed to construct the wideband MN, whose topology and circuit parameters are acquired through optimization. Finally, the impedance realized by the designed MN falls into the target impedance region obtained by using multi-harmonic bilateral pull technique in the desired frequency band. For the proof of the method, a broadband highly efficient PA has been designed, fabricated, and measured using commercialized GaN high electron mobility transistors (HEMT). The measured results show that the implemented PA achieves a bandwidth of 137.8% from 0.7 to 3.8 GHz. The drain efficiency is between 59% and 70% with an output power of greater than 39 dBm and a gain ranging from 9 to 12.1 dB.

## Introduction

With the arrival of the 5 G communication era, more requirements are put forward for communication systems. As the most important part of a radio frequency (RF) transceiver, power amplifiers (PAs) with wider bandwidth and higher efficiency have become a research hot spot [1–6].

The difficulty of realizing high efficiency in a wide frequency band lies in the fact that the optimal impedance of the input and output terminals of transistors has an impedance dispersion effect where the impedance varies with the operating frequency. In addition, the optimal impedance matching can only be achieved at a single frequency point based on the conventional impedance matching theory. Therefore, many different circuit structures and methods have been proposed to expand operating bandwidth, such as distributed PAs, a series of continuous modes, and extended continuous mode PAs [7–9].

Among them, the distributed PA has outstanding capabilities in improving bandwidth, but the efficiency is normally in the range of 20–30% [10]. Coincidentally, in order to improve the operation efficiency of the PAs, distributed matching network (MN) [11, 12] with harmonic manipulation has also been successively proposed, which also includes dual-band impedance matching, but is still limited in bandwidth expansion. The new operation modes represented by the extended continuous Class-F [13–15] and extended continuous Class-B/J [16–18] PAs can extend the impedance of the second harmonic to a resistive-reactive state to realize the design of the broadband PAs. However, these methods achieve a wideband at the expense of operating efficiency, which is attributed to the fact that the impedance matching method has never broken through the limitation of single frequency point matching.

Driven by the application demand, to solve the problem that the performance of the PA is limited due to single frequency point matching, a method of realizing wideband matching by algorithm optimization has emerged. Several optimization-based methods based on filter-based network synthesis [19, 20] or real-frequency technique [21] have been proposed. Nevertheless, the distributed MNs cannot be directly acquired, which means they need to be transformed into a distributed network to be realized. The conversion from lumped elements to transmission lines will introduce errors, which need to be optimized in the later stages to reduce the errors caused by the conversion. This will undoubtedly increase the complexity and uncertainty of MN design.

In this paper, a novel technique to realize impedance MN directly by transmission line is proposed, in which the topology and circuit parameters are determined through optimization. The designed PA based on the proposed approach exhibits excellent efficiency performance with a more than two-octave operation bandwidth. The rest of this letter is organized as follows: the section "Design of the principle of the output matching network" presents

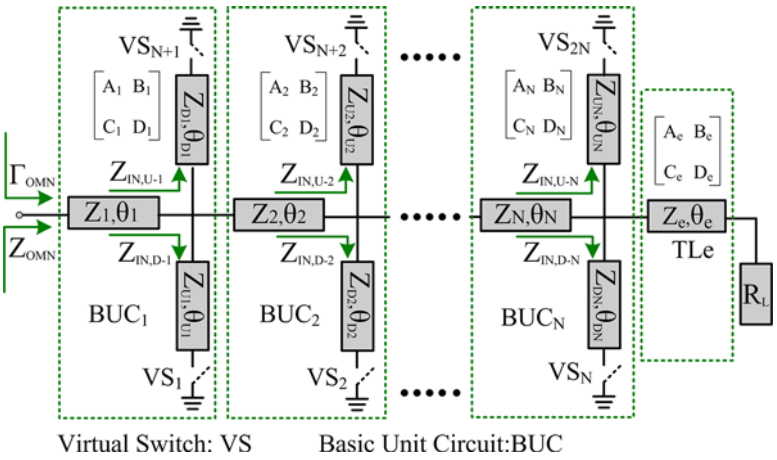


**Figure 1.** A schematic diagram of the proposed distributed matching network.

the analysis of the proposed output MN using optimization to obtain the topology and circuit parameters of the distributed left-rotating T-type structure. Then, the implementation process of wideband highly efficient PA is given in the section "Realization of wideband highly efficient PA". For validation, measured results are shown in the section "Implementation and measurements". Finally, a conclusion is given in the section "Conclusion".

## Design of the principle of the output matching network

Considering that the proposed PA needs to expand bandwidth while maintaining high efficiency, the selection of impedance MN is particularly important. By summarizing the existing impedance matching topology, a variable universal output MN is proposed. The topological network formed by this universal structure can almost cover all the existing structures with any number of branches and impedance gradient matching. The proposed output MN topology with the left-rotating T-type structure as the basic unit circuit (BUC) for cascading is shown in Fig. 1, where the number of cascades is determined by optimization. This BUC is composed of a series microstrip line and two shunt stubs connected to the ground through a virtual switch (VS), where the shunt stubs are presented as open or short stubs depending on the state of the VS. It can be clearly seen that the proposed topology contains $N$ BUCs and $2N$ VS. Each form of composition has different responses, which provides great flexibility for MN design. Therefore, the performance of the designed MN is basically determined by the number of $\mathrm{BUC_{si}}$ $(1 \le i \le N)$ and the opening or closing of $\mathrm{VS}_i$ $(1 \le i \le 2N)$.

The most basic approach to measuring the performance of impedance matching is to evaluate the closeness between the impedance realized by MN and the target impedance at the corresponding design frequency point. In view of this, obtaining the expression of input impedance $Z_{\mathrm{OMN}}$ becomes a key point. The feasible way is to first acquire the transmission matrix $\mathbf{A}_i$ suitable for describing each basic left-rotating T-type unit of the cascade network, then conduct cascade multiplication, and finally convert it into a scattering matrix. Based on the above analysis, the ABCD matrix of BUCs in Fig. 1 can be expressed as follow (1):

$$\mathbf{A}_i = \begin{bmatrix} \cos(\theta_i) + \frac{j\cdot(Z_{\mathrm{IN},U-i}+Z_{\mathrm{IN},D-i})Z_i\sin(\theta_i)}{Z_{\mathrm{IN},U-i}\cdot Z_{\mathrm{IN},D-i}} & j\cdot Z_i\sin(\theta_i) \\ \frac{j\cdot\sin(\theta_i)}{Z_i} + \frac{(Z_{\mathrm{IN},U-i}+Z_{\mathrm{IN},D-i})\cdot\cos(\theta_i)}{Z_{\mathrm{IN},U-i}\cdot Z_{\mathrm{IN},D-i}} & \cos(\theta_i) \end{bmatrix} \quad 1 \le i \le N, \tag{1}$$

where $Z_i$ and $\theta_i$ are the characteristic impedances and electrical length of the series lines, respectively; $Z_{\mathrm{IN},U\text{-}i}$ and $Z_{\mathrm{IN},D\text{-}i}$ are the input impedances of the two shunt stub of the $i$th BUCs, respectively, and can be calculated as follows:

$$\begin{cases} Z_{\mathrm{IN},D-i} = \overline{\mathrm{VS}_i}\cdot jZ_{Ui}\cdot\tan(\theta_{Ui}) + \frac{\mathrm{VS}_i}{jZ_{Ui}\cdot\tan(\theta_{Ui})} \\ Z_{\mathrm{IN},U-i} = \overline{\mathrm{VS}_{N+i}}\cdot jZ_{Di}\cdot\tan(\theta_{Di}) + \frac{\mathrm{VS}_{N+i}}{jZ_{Di}\cdot\tan(\theta_{Di})} \end{cases} \quad 1 \le i \le N, \tag{2}$$

where $Z_{Ui}$ and $Z_{Di}$ are the characteristic impedances of the two shunt stub lines, respectively; $\theta_{Ui}$ and $\theta_{Di}$ are the electrical lengths of the two shunt stub lines, respectively; $\mathrm{VS}_i$ $(1 \le i \le 2N)$ represents the on and off states of the $i$th VS, which can be defined as

$$\mathrm{VS}_i = \mathrm{VS}_{N+i} = \begin{cases} 0 & \mathrm{ON} \\ 1 & \mathrm{OFF} \end{cases} \quad 1 \le i \le N. \tag{3}$$

The output MN can be treated as a cascaded structure of $N$ BUCs interconnected with a load impedance $R_{\mathrm{L}}$. Considering the electric length $\theta$ as a function of frequency, the ABCD matrix of the output MN can be expressed as follow (4):

$$\begin{aligned} \mathbf{A} &= \left[\prod_{N}^{i=1} A_i(f)\right]\cdot\begin{bmatrix} \cos(\theta_e) & jZ_e\sin(\theta_e) \\ \frac{jZ_e\sin(\theta_e)}{Z_e} & \cos(\theta_e) \end{bmatrix} \\ &= \begin{bmatrix} A_T(f) & B_T(f) \\ C_T(f) & D_T(f) \end{bmatrix}_{\mathrm{Total}} \quad 1 \le i \le N, \end{aligned} \tag{4}$$

where $Z_e$ and $\theta_e$ represent the characteristic impedances and electrical length of the transmission line $\mathrm{TL}_e$, respectively.

The ABCD parameters of the proposed output MN are acquired and can be easily transformed to scattering parameters [22]. The output MN can be regarded as a two-port network, so the scattering matrix should include four parameters: $S_{11}(f)$, $S_{12}(f)$, $S_{21}(f)$, and $S_{22}(f)$. It needs to be noted that if the characteristic impedance $Z_e$ of $\mathrm{TL}_e$ is equal to the load impedance $R_{\mathrm{L}}$, the following equation can be satisfied.

$$\Gamma_{\mathrm{OMN}}(f) = S_{11}(f), \tag{5}$$

where $\Gamma_{\mathrm{OMN}}$ is the reflection coefficient of the output MN, and the input impedance $Z_{\mathrm{OMN}}$ can be expressed as

$$Z_{\mathrm{OMN}}(f) = Z_1\frac{1+\Gamma_{\mathrm{OMN}}(f)}{1-\Gamma_{\mathrm{OMN}}(f)}. \tag{6}$$

https://doi.org/10.1017/S1759078723000314 Published online by Cambridge University Press

To achieve wideband high-efficiency performance of PAs, it is necessary to ensure that $Z_{OMN}$ is close to the target impedance in the desired bandwidth. To this end, the cost function in an optimization procedure [23] is taken as follows:

$$T = \sum_{K}^{i=1} \left| \frac{Z_{OMN}(f_i) - Z_{OPT}(f_i)}{Z_{OPT}(f_i)} \right|^2. \quad (7)$$

Hence, the optimization objective can be defined as (7), where $Z_{OPT}$ is the optimal impedance, which can be acquired by load-pull technology, and $f_i$ (where $i = 1, 2, \ldots, k$) are frequency points within the desired bandwidth. As a result, the output matching topology can be determined through optimization.

## Realization of wideband highly efficient PA

In this brief, the desired specifications are stated as follows: A wideband highly efficient PA is designed in a target operating frequency band of 0.8–3.9 GHz. To achieve the design goals, a 10-W GaN HEMT device CGH40010F is selected and the static bias points are set at $V_{GS} = -2.7$ V and $V_{DS} = 28$ V.

### *Acquisition of optimal impedance*

Considering that the harmonic component has a great impact on the output power and efficiency, it is necessary to analyze the harmonic component in the design process of PA. For the typical PA design, the conventional load-pull technique is used to obtain the fundamental impedance, while the influence of harmonic impedance is ignored. Therefore, in the design of ultra-wideband PA, there is a deviation in impedance matching, which limits the performance of PA bandwidth and efficiency.

In order to comprehensively analyze the influence of harmonic impedance on the performance of the PA, especially the second harmonic, the multi-harmonic bilateral pull technique [24] is used to obtain the optimum fundamental and second harmonic impedance.

Based on the transistor large signal model provided by Cree, optimal fundamental and second harmonic impedance regions of the load for 1.0 to 4.0 GHz demonstrated in Fig. 2(a) are generated by employing the multi-harmonic bilateral pull technique at the output terminals. It is worth noting that the internal region of the impedances of the fundamental and second harmonic contours represents the tolerable region in which high efficiency and high output power can be acquired.

Moreover, it can be observed from Fig. 2(a) that when the second harmonic resistance within the entire desired frequency band is maintained between 0 and 25 Ω, higher than $\eta_{max}$-5% efficiency and $P_{max}$-3 dBm output power can be obtained. Meanwhile, when the second harmonic reactance is maintained between 0 and 55 Ω, higher than $\eta_{max}$-3% efficiency and $P_{max}$-2 dBm output power can also be achieved. Therefore, based on the above analysis, a conclusion can be drawn that when the second harmonic impedance is extended to a resistive-reactive and partially overlaps with the optimal fundamental impedance region, excellent performance can still be achieved. As a result, especially, the second harmonic in the frequency band can be incorporated into the optimal fundamental impedance region, thus making it possible to realize a multifrequency high-efficiency PA.

Furthermore, it can be clearly seen from Fig. 2(a) that across a wide bandwidth, the optimum fundamental impedances of a transistor at different frequency points are not close to each other.

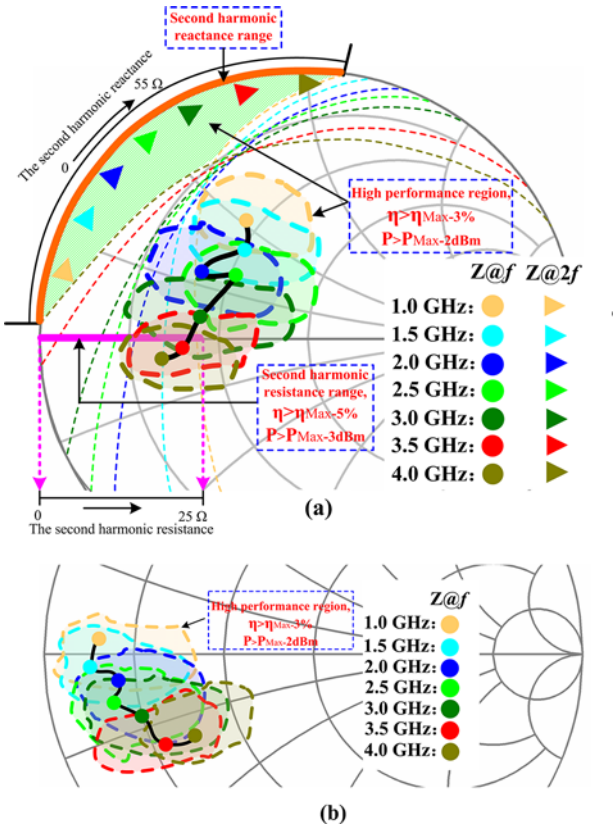


**Figure 2.** The optimal fundamental impedance distribution of (a) load and (b) source for 1.0–4.0 GHz.

Therefore, the entire operating bandwidth is divided into seven frequency sections depending on the required bandwidth and the variation of the optimal impedances. For each frequency section, the region with high output power and high-efficiency contours can be selected as the optimum fundamental impedance of the frequency section. Similarly, the optimal impedance of the input terminals is also shown in Fig. 2(b).

### *Realization of input and output matching network*

As the optimal impedance region is determined, the design theory presented in the second section can be employed to acquire an appropriate topology. Then, the variable $K$ described in (7) takes the value 7. Figure 3(a) depicts the implemented topology for output matching, which is based on the Rogers 4350B microstrip transmission line with a thickness of 0.762 mm. Similarly, based on the output MN synthesized, the input MN is also proposed by using a similar method, as shown in Fig. 3(b).

As a consequence, the wideband highly efficient GaN HEMT PA including input and output MN achieved by using transmission lines is demonstrated in Fig. 4. It should be noted that since the designed frequency band exceeds one octave, considering the in-band stability, a stability network comprising of the parallel RC pair of 9 pF and 3 ohms is specially added to the input terminal. Especially, the gate bias resistors perform low frequency stabilization.

Moreover, to better evaluate whether $\Gamma_S$ and $\Gamma_{OMN}$ realized by the designed input and output MN are close to the optimal impedance region, the source and load impedance

https://doi.org/10.1017/S1759078723000314 Published online by Cambridge University Press

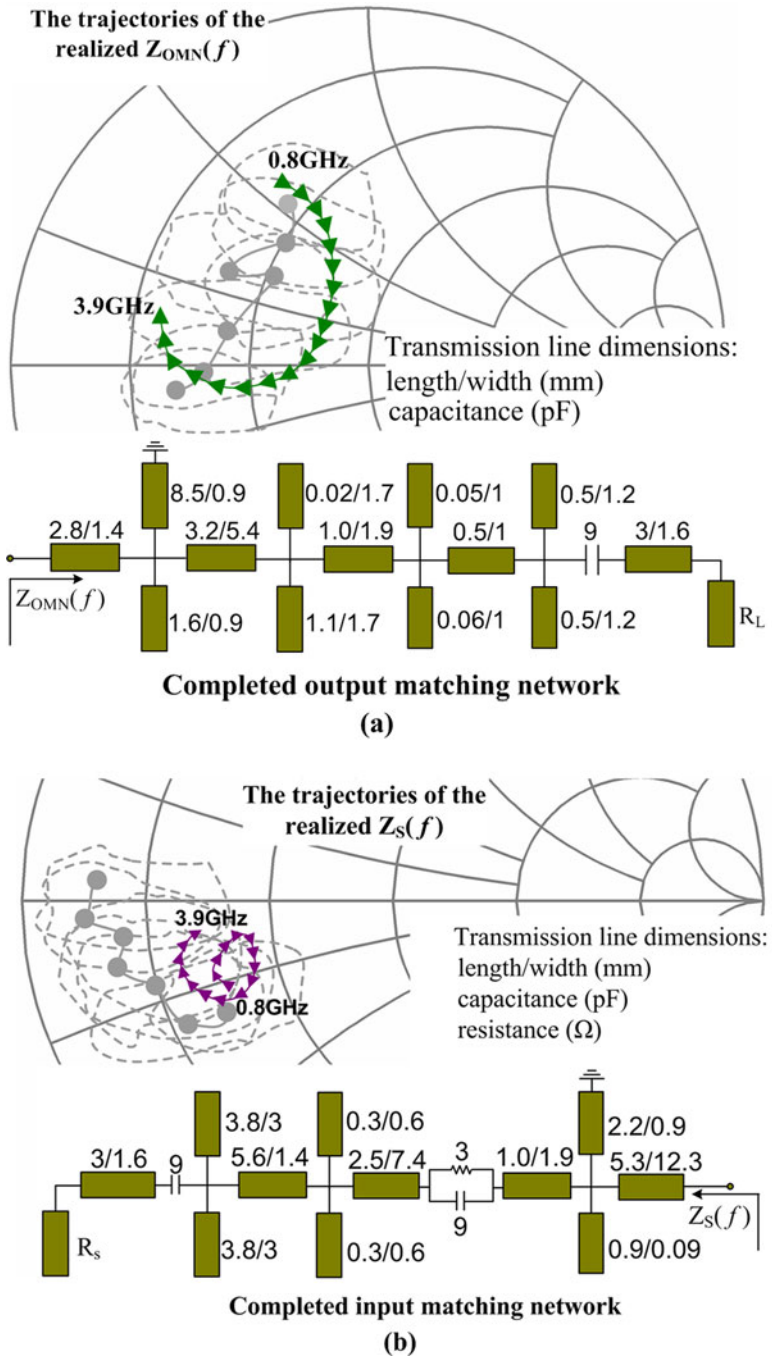


**Figure 3.** The completed output (a) and input (b) matching network. The trajectories of the realized $Z_{OMN}(f)$ and $Z_S(f)$.

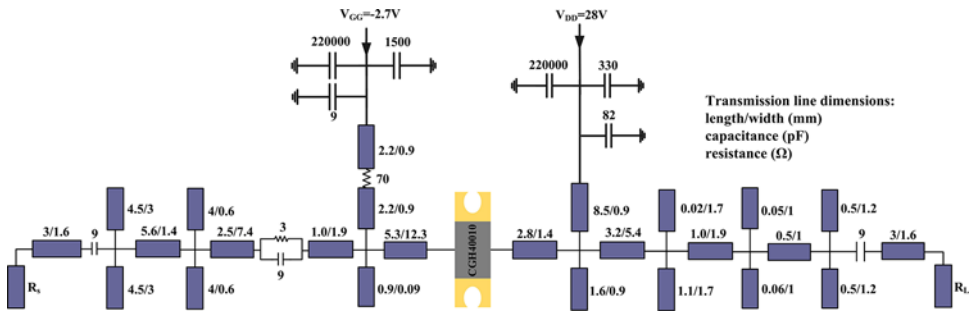


**Figure 4.** The final schematic of the proposed multioctave bandwidth PA.

https://doi.org/10.1017/S1759078723000314 Published online by Cambridge University Press

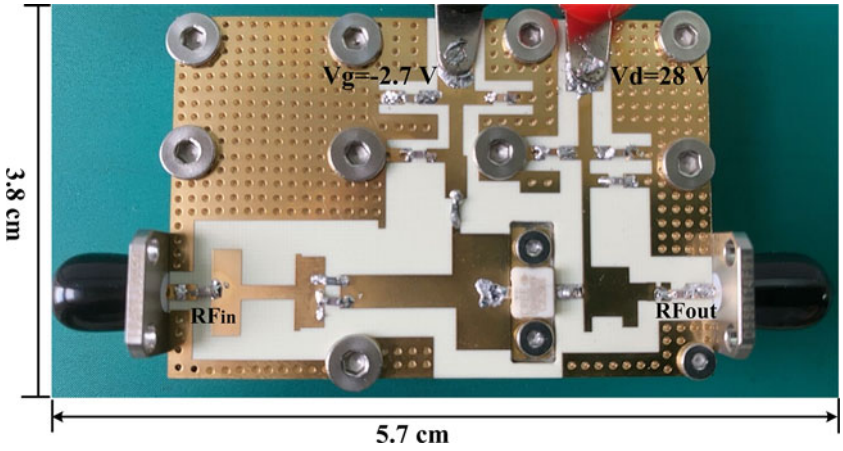


**Figure 5.** The photograph of the fabricated PA.

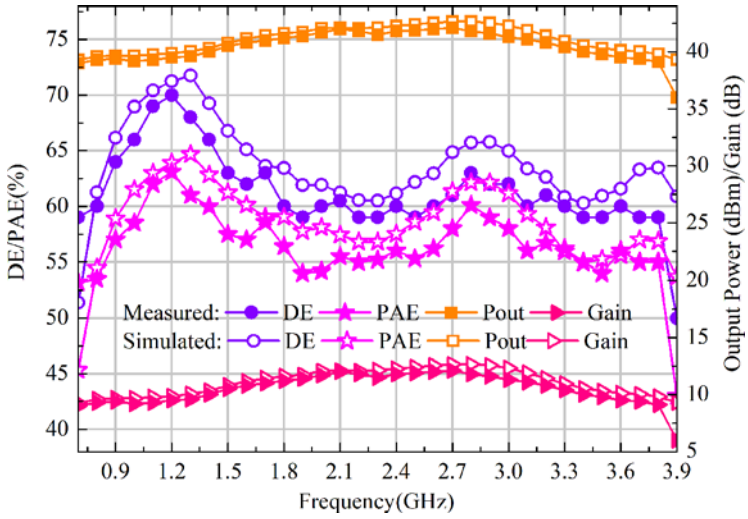


**Figure 6.** Measured and simulated DE, PAE, output power, and gain across the entire bandwidth.

trajectories obtained by using simulation software are plotted in Fig. 3(a) and (b). From Fig. 3(a), it can be clearly observed that the trajectories of load impedance $\Gamma_{OMN}(f)$ are represented by a curve composed of cyan solid triangles. Starting from 0.8 GHz, with the increase of frequency, it gradually moves down from the upper right corner of the Smith chart and ends at 3.9 GHz. It is obvious that the impedance trajectories basically fall into the target impedance region, which is the gray-shaded dashed background. In addition, the trajectories of the source impedance $\Gamma_S(f)$ (purple triangle curve) are depicted in Fig. 3(b). It is evident that the impedance curve from 0.8 to 3.9 GHz is well manipulated in a small area where the target impedance is located. Therefore, the above simulation results reveal the fact that the proposed design theory is superior.

## Implementation and measurements

The photograph of the fabricated wideband highly efficient PA with a size of 3.8 × 5.7 cm$^2$ is presented in Fig. 5.

To verify the proposed design theory and evaluate the performance of the assembled PA, continuous wave is generated by the signal generator from 0.7 to 3.9 GHz with a 0.1 GHz step to implement the PA measurement. Figure 6 demonstrates that from the operating bandwidth of 0.7–3.8 GHz with a relative bandwidth of 137.8%, the drain efficiency (DE) between 59% and 70%, the power added efficiency (PAE) of 53.2%–63.1%, the output power of 39–42.1 dBm, and the gain of 9–12.1 dB are achieved under the condition of maintaining the input power of 30 dBm. From the measured performance of the PA, the measured and simulated results are basically consistent, and the rationality of the proposed theory is proved again. In addition, it is worth noting that there are some deviations between simulation and measurement results in terms of efficiency, output power, and operating bandwidth, which is mainly reflected in the deterioration of the measured results at 3.9 GHz compared with the simulation results, but good performance at 0.7 GHz. The possible causes of this phenomenon are attributed to the assembly tolerance, simulation model error, and electromagnetic coupling of practical circuits.

The measured DE gain versus the corresponding input power at seven frequency points of 0.8, 1.0, 1.5, 2.0, 2.5, 3.0, and 3.5 GHz is drawn in Fig. 7. It can be seen from the figure that when the gain is compressed by 3 dB in the 0.7–3.8 GHz range, the output power has reached a saturation and the DE can reach 59–70%.

A summary of some recently reported broadband high-efficiency PAs is presented in Table 1. To facilitate comparison between the proposed PA and the other relevant designs, the proposed PA measurement results are also given in Table 1. It is

https://doi.org/10.1017/S1759078723000314 Published online by Cambridge University Press

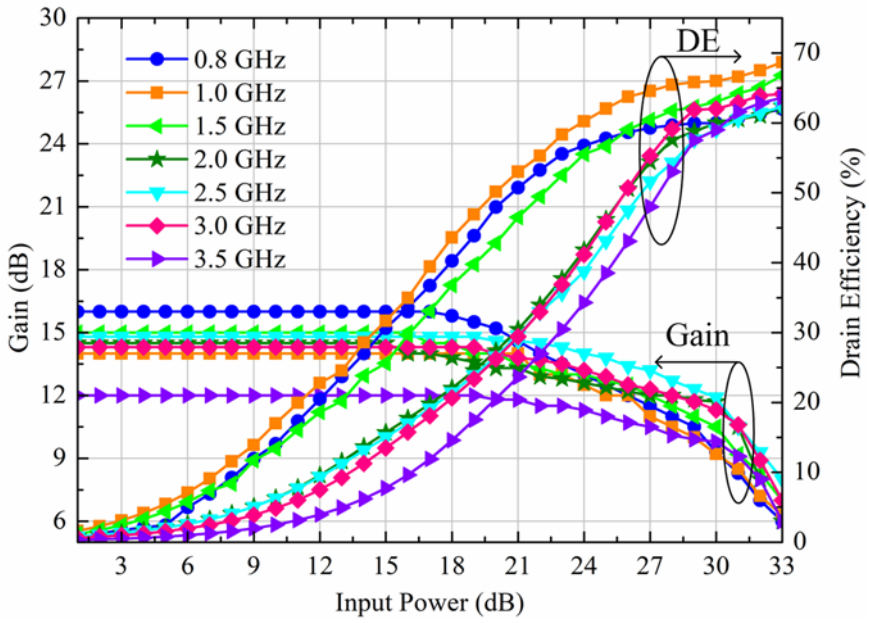


**Figure 7.** Measured DE and gain versus input power at different operating frequencies.

**Table 1.** Comparisons with state-of-the-art broadband PAs

| Reference | BW (GHz) | RBW (%) | DE (%) | Power (dBm) | Gain (dB) | Year |
|---|---|---|---|---|---|---|
| [25] | 1.8–2.7 | 40 | 48–65.2[a] | 42.4–44.62 | ≥8 | 2018 |
| [26] | 0.5–3.15 | 145.2 | 58–74.9 | 39.03–42.87 | 8.43–15.67 | 2020 |
| [27] | 0.8–3.2 | 120 | 57–74 | 39.7–42.9 | 10.7–14.1 | 2018 |
| [28] | 2.4–4.6 | 62.8 | 51–70 | 40–42.8 | 12.8–14.9 | 2021 |
| [29] | 3.3–4.3 | 26 | 64–68 | 39.5–40.3 | 16.5–17.3 | 2022 |
| This work | 0.7–3.8 | 137.8 | 59–70 | 39–42.1 | 9–12.1 | 2022 |

[a] PAE.
BW: bandwidth, RBW: relative bandwidth.

obvious that the proposed PA has greatly expanded its operating bandwidth and relative bandwidth while maintaining high DE.

## Conclusion

In this paper, the design process, fabrication, and measurement of a wideband highly efficient PA is presented. The multi-harmonic bilateral pull technique is employed to acquire the optimum impedances of fundamental and second harmonic, and the impedance region of the second harmonic is analyzed to find that the second harmonic impedance can be extended to a resistive-reactive. The MN is constructed by using distributed network cells with a left-rotating T-type structure through optimization to achieve impedance matching within the desired bandwidth. As a verification, the proposed PA is implemented and fabricated by employing GaN HEMT transistors. The measured results show that a good performance is obtained. The DE can reach 59–70% and an output power greater than 39 dBm can be realized in the operating bandwidth of 0.7–3.8 GHz.

**Financial Support.** The work was proposed by the Project of Ministry of Science and Technology (grant 2018YFE0207500 and grant D20011), the National Natural Science Foundation (grant 61871169 and grant 62201181), the Zhejiang Provincial Natural Science Foundation (grant LZ20F010004), the General Project of Huainan Normal University (grant 2021XJYB026), the Huainan Guiding Science and Technology Plan Project (grant 2021001), University Natural Science Foundation of Anhui Province (grant 2022AH051578), and the Science and Technology Plan Project of HuaiNan, China (grant 2021A2411).

**Competing interests.** We declare that the authors have no competing interests as defined by *International Journal of Microwave and Wireless Technologies* or other interests that might be perceived to influence the results and/or discussion reported in this paper. The authors report no conflict of interest.

## References

1. **Liu C, Li X, Zhao Y, Qi T, Du X, Chen W and Ghannouchi FM** (2021) Investigation of high-efficiency parallel-circuit class-EF power amplifiers with arbitrary duty cycles. *IEEE Transactions on Industrial Electronics* **68**(6), 5000–5012.
2. **Yang Z, Li M, Dai Z, Xu C, Jin Y, Li T and Tang F** (2020) A generalized high-efficiency broadband class-E/F 3 power amplifier based on design space expanding of load network. *IEEE Transactions on Microwave Theory and Techniques* **68**(9), 3732–3744.
3. **Feng W, Zhou XY, Che W and Shi Y** (2022) Broadband high-efficiency quasi-class-j power amplifier based on nonlinear output capacitance effect. *IEEE Transactions on Circuits and Systems II: Express Briefs* **69**(4), 2091–2095.
4. **Moshfegh M and Miar-Naimi H** (2022) High-efficiency broadband Class-E PAs for more than one octave: Analysis and design. *IEEE Transactions on Microwave Theory and Techniques* **70**(7), 3534–3547.
5. **Nia HT-A and Nayyeri V** (2018) A 0.85-5.4 GHz 25-W GaN Power amplifier. *IEEE Microwave and Wireless Components Letters* **28**(3), 251–253.
6. **Colantonio P, Giannini F, Giofrè R and Piazzon L** (2008) High efficiency ultra-wide-band power amplifier in GaN technology. *Electronics Letters* **44**(2), 130–131.
7. **Yang M, Xia J, Guo Y and Zhu A** (2016) Highly efficient broadband continuous inverse class-F power amplifier design using modified elliptic low-pass filtering matching network. *IEEE Transactions on Microwave Theory and Techniques* **64**(5), 1515–1525.

https://doi.org/10.1017/S1759078723000314 Published online by Cambridge University Press

8. **Zhang Z, Liu G, Liu G and Li S** (2020) Design of a broadband high-efficiency hybrid class-EFJ power amplifier. *IEEE Microwave and Wireless Components Letters* **30**(4), 407–409.
9. **Latha YMA and Rawat K** (2022) Design of ultra-wideband power amplifier based on extended resistive continuous Class B/J mode. *IEEE Transactions on Circuits and Systems II: Express Briefs* **69**(2), 419–423.
10. **Kumar N and Grebennikov A** (2015) *Distributed Power Amplifiers for RF and Microwave Communications*. Norwood, MA: Artech House.
11. **Colantonio P, Giannini F, Giofrè R and Piazzon L** (2008) Design technique for concurrent dual band harmonic tuned power amplifier. *IEEE Transactions on Microwave Theory and Techniques* **56**(11), 2545–2555.
12. **Giannini F and Scucchia L** (2009) A complete class of harmonic matching networks: Synthesis and applications. *IEEE Transactions on Microwave Theory and Techniques* **57**(3), 612–619.
13. **Eskandari S and Kouki AB** (2022) The second source harmonic optimization in continuous Class-GF power amplifiers. *IEEE Microwave and Wireless Components Letters* **32**(4), 316–319.
14. **Huang H, Zhang B, Yu C, Gao J, Wu Y and Liu Y** (2017) Design of multioctave bandwidth power amplifier based on resistive second-harmonic impedance continuous Class-F. *IEEE Microwave and Wireless Components Letters* **27**(9), 830–832.
15. **Zheng SY, Liu ZW, Zhang XY, Zhou XY and Chan WS** (2018) Design of ultrawideband high-efficiency extended continuous Class-F power amplifier. *IEEE Transactions on Industrial Electronics* **65**(6), 4661–4669.
16. **Xuan X, Yang F and Liu C** (2019) Design of multioctave high-efficiency power amplifier based on extended continuous Class-B/J modes. *International Journal of RF and Microwave Computer-Aided Engineering* **29**(10), 1–12.
17. **Du X, You CJ, Cai J, Helaoui M, Ghannouchi FM, Zhao Y and Li X** (2018) Novel design space of load modulated continuous class-B/J power amplifier. *IEEE Microwave and Wireless Components Letters* **28**(2), 156–158.
18. **Friesicke C, Quay R and Jacob AF** (2015) The resistive-reactive class-J power amplifier mode. *IEEE Microwave and Wireless Components Letters* **25**(10), 666–668.
19. **Xia J, Zhu X and Zhang L** (2014) A linearized 2–3.5 GHz highly efficient harmonic-tuned power amplifier exploiting stepped-impedance filtering matching network. *IEEE Microwave and Wireless Components Letters* **24**(9), 602–604.
20. **Chen K and Peroulis D** (2012) Design of broadband highly efficient harmonic-tuned power amplifier using in-band continuous class-F–1/F mode transferring. *IEEE Transactions on Microwave Theory and Techniques* **60**(12), 4107–4116.
21. **Lu Z and Chen W** (2013) Resistive second-harmonic impedance continuous Class-F power amplifier with over one octave bandwidth for cognitive radios. *IEEE Journal on Emerging and Selected Topics in Circuits and Systems* **3**(4), 489–497.
22. **Frickey DA** (1994) Conversions between S,Z,Y,H, ABCD, and T parameters which are valid for complex source and load impedances. *IEEE Transactions on Microwave Theory and Techniques* **42**(2), 205–211.
23. **Dai Z, He S, You F, Peng J, Chen P and Dong L** (2015) A new distributed parameter broadband matching method for power amplifier via real frequency technique. *IEEE Transactions on Microwave Theory and Techniques* **63**(2), 449–458.
24. **Chen H and Zhang YX** (2008) Design of microwave power amplifier based on multi-harmonic bilateral-pull technology. *Journal of Microwaves* **24**(3), 57–60.
25. **Sharma T, Aflflaki P, Helaoui M and Ghannouchi FM** (2018) Broadband GaN class-E power amplifier for load modulated delta sigma and 5G transmitter applications. *IEEE Access* **6**, 4709–4719.
26. **Chen H, Xu J-X, Kong ZH, Chen W-H and Zhang XY** (2020) Broadband high-efficiency power amplifier with quasi-elliptic low-pass response. *IEEE Access* **8**, 52566–52574.
27. **Wang J, He S, You F, Shi W, Peng J and Li C** (2018) Codesign of high efficiency power amplifier and ring-resonator filter based on a series of continuous modes and even-odd-mode analysis. *IEEE Transactions on Microwave Theory and Techniques* **66**(6), 2867–2878.
28. **Poluri N and De Souza MM** (2021) Designing a broadband amplifier without load-pull. *IEEE Microwave and Wireless Components Letters* **31**(6), 593–596.
29. **Eskandari S and Kouk AB** (2022) The second source harmonic optimization in continuous class-GF power amplifiers. *IEEE Microwave and Wireless Components Letters* **32**(4), 316–319.


**Xuefei Xuan** received the M.E. degrees in electromagnetic field and microwave techniques from the Hangzhou Dianzi University, Hangzhou, Zhejiang, China, in 2018. He is currently pursuing the Ph.D. degree with the Hangzhou Dianzi University, Hangzhou, and works with the School of Electronic Engineering, Huainan Normal University, Huainan, China. His research interests include the design of RF/mm-wave power amplifiers, efficiency enhancement techniques, broadband techniques, and mm-wave integration circuits and systems.

**Zhiqun Cheng** received the B.S. and M.S. degrees from the Hefei University of Technology, Hefei, China, in 1986 and 1995, respectively, and the Ph.D. degree in microelectronics and solid state electronics from the Shanghai Institute of Metallurgy, Chinese Academy of Sciences, Shanghai, China, in 2000. From 1986 to 1997, he was a Teaching Assistant and a Lecturer with the Hefei University of Technology, China. From 2000 to 2005, he was an Associate Professor with the Shanghai Institute of Metallurgy, China. He is currently a Professor and the Dean of the School of Electronic and Information, Hangzhou Dianzi University. He has authored or co-authored over 150 technical journals and conference papers. His research interests include microwave theory and technology, MMIC, power amplifier, and RF front end. He is currently a member of a Council of Zhejiang Electronic Society. He was also a Chair of the Organizational Committee for over 10 International Conferences.

**Zhiwei Zhang** received the B.S. degree in electronic science and technology from the Hangzhou Dianzi University, Hangzhou, China, in 2017, where he is currently pursuing the Ph.D. degree with Key Laboratory of RF Circuit and System, Education Ministry. He is currently with the Centre for Wireless Innovation, ECIT Institute, Queen's University Belfast, as a visiting student. His current research interests include highly linear and efficient microwave PA design.

**Tingwei Gong** is currently pursuing the Ph.D. degree with Key Laboratory of RF Circuit and System, Education Ministry. He is currently with the Centre for Wireless Innovation. His research interests include microwave theory and technology, MMIC, power amplifier, and RF front end.

**Chao Le** is currently the project leader of Fuyang Electronic Information Research Institute Co., Ltd., of the Hangzhou University of Electronic Science and Technology.

https://doi.org/10.1017/S1759078723000314 Published online by Cambridge University Press